Soft Matter

Quantitative mechanical analysis of indentations on layered, soft elastic materials

Journal:	*Soft Matter*
Manuscript ID	SM-ART-10-2018-002121.R1
Article Type:	Paper
Date Submitted by the Author:	20-Dec-2018
Complete List of Authors:	Doss, Bryant; Arizona State University, Physics Rahmani Eliato, Kiarash; Arizona State University Department of Physics Lin, Keng-hui; Academia Sinica, Physics Ros, Robert; Arizona State University, Physics

Quantitative mechanical analysis of indentations on layered, soft elastic materials

Bryant L. Doss[a,b,§,*], Kiarash Rahmani Eliato[a,b,c], Keng-hui Lin[d], and Robert Ros[a,b,c,*]

[a]Department of Physics, Arizona State University, Tempe, AZ 85287, USA

[b]Center for Biological Physics, Arizona State University, Tempe, AZ 85287, USA

[c]Biodesign Institute, Arizona State University, Tempe, AZ 85281, USA

[d]Institute of Physics, Academia Sinica, Taipei 11529, Taiwan

[§]Present address: Mechanobiology Institute, National University of Singapore, Singapore 117411, Singapore

*correspondence: bryantdoss@gmail.com (B.L.D.), robert.ros@asu.edu (R.R.)

Abstract

Atomic force microscopy (AFM) is becoming an increasingly popular method for studying cell mechanics, however the existing analysis tools for determining the elastic modulus from indentation experiments are unable to quantitatively account for mechanical heterogeneity commonly found in biological samples. In this work, we numerically calculated force-indentation curves onto two-layered elastic materials using an analytic model. We found that the effect of the underlying substrate can be quantitatively predicted by the mismatch in elastic moduli and the homogeneous-case contact radius relative to the layer height for all tested probe geometries. The effect is analogous to one-dimensional Hookean springs in series and was phenomenologically modeled to obtain an approximate closed-form equation for the indentation force onto a two-layered elastic material which is accurate for up to two orders of magnitude mismatch in Young's modulus when the contact radius is less than the layer height. We performed finite element analysis simulations to verify the model and AFM

microindentation experiments and macroindentation experiments to demonstrate its ability to deconvolute the Young's modulus of each layer. The model can be broadly used to quantify and serve as a guideline for designing and interpreting indentation experiments into mechanically heterogeneous samples.

Introduction

Indentation-based elasticity measurements are commonly used to investigate mechanical properties of materials across many length, time, and rigidity scales.[1] A frequently used tool for active micro- and nanoindentation is the atomic force microscope (AFM), allowing for the characterization of materials with various probe geometries with multiple magnitudes of dimensions (10^{-9}-10^{-5} m) and forces (10^{-12}-10^{-6} N). AFM indentation has been applied at the nanometer scale to quantify mechanical properties of microtubules,[2] viruses,[3, 4] polymer films,[5] hydrogels,[6-9] and is being increasingly used in the fields of cell mechanics[10-18] and tissue mechanics.[19, 20] The basic principle is to indent an object with a probe of known geometry and dimensions and measure the force of indentation as a function of distance into the sample, producing a force-indentation (F-δ) curve. Nominally, these F-δ curves may be fit to an elastic contact model, such as Hertz[21] or Sneddon[22], to determine the Young's (or elastic) modulus E of the sample when the Poisson's ratio ν is known (for a detailed review, see Ref. [23]). ν is typically between 0 and 0.5 and assumed to be 0.5 for rubber-like materials. Assumptions of these models include that the sample is an infinite half-space with homogeneous, isotropic elasticity with no viscosity, there is frictionless, non-adhesive contact between the surface and the probe, and the strains are small; most samples encountered in cell and tissue mechanics do not meet these assumptions.

One common problem is the presence of some mechanical heterogeneity in the sample, for example a thin cell[24] or the actin cortex of a cell,[25] which may be modeled as a thin elastic layer that is supported by a substrate with different mechanical properties. Elastic contact models have been extended to account for the effects of an infinitely rigid substrate for axially symmetric probe geometries.[26-28] Other models have been developed to account for a thin layer that has a small (less than one magnitude) elastic mismatch to its substrate,[29-31] define an equivalent elastic modulus for a multi-layered system using a numeric approach,[32, 33] use a mixed finite element analysis approach,[34] or for cells specifically to treat the top layer as an entropic polymer brush and the cell body an elastic sample[35] or add additional contribution arising from surface tension.[36] However, the field lacks a simple formulation that may be easily applied to any elastic mismatch between two elastic layers for all probe geometries. In this article we present a method for the mechanical quantification of elastic, layered materials, which has general application to many probe geometries and sample types. Further, it allows to estimate the influence of underlying materials to force-indentation curves and therewith the resulting Young's moduli. Finite element simulations are performed to validate the approach, and AFM microindentation and macroindentation experiments are performed to assess the applicability of the model.

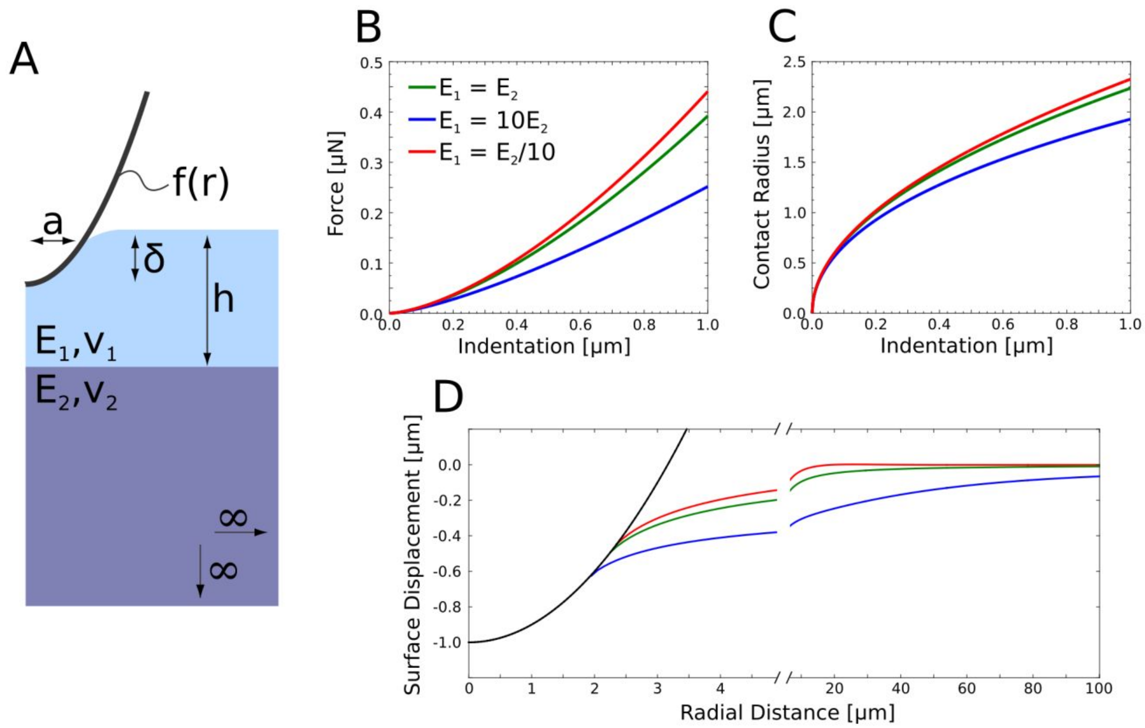

Figure 1: Overview of the bonded two-layer axisymmetric indentation model. (A) Illustration of the model with the relevant physical parameters. (B) Force-indentation curves calculated from the numeric model for three cases: the homogeneous case (green), a stiffer substrate (red), and a softer substrate (blue). (C) Contact radius between the indenter and surface of the indentation as a function of indentation depth. (D) Surface displacement profile calculated from Eq. 10. Parameters used to calculate are: parabolic indenter geometry (Hertz model), R=5 μm, h=20 μm, E_1=100 kPa, E_2=100 kPa, 10kPa, or 1MPa for green, blue, and red, respectively, $\nu_1=\nu_2=0.5$, and in (D) δ=1.0 μm.

Sneddon demonstrated that the axisymmetric elastic indentation problem in cylindrical coordinates can be reduced using Hankel Transforms into a dual integral problem to solve for the stress-strain relations along the deformed surface of an infinite half-space.[22] From this, F-δ relations can be derived for any arbitrary indenter geometry defined by a function f. Dhaliwal and Rau extended the work of Sneddon to include an elastic layer bonded to an infinite elastic half-space (Fig. 1A) by imposing additional boundary conditions between the two elastic layers.[37] The F-δ relations are determined by solving a Fredholm Integral Equation of the Second Kind:[37, 38]

$$\phi(t) + \frac{a}{h\pi}\int_0^1 K(x,t)\phi(x)dx = -\frac{E_1 a}{2(1-{\nu_1}^2)}[\delta - \beta(t)] \quad (1)$$

$$F = -4\int_0^1 \phi(t)dt \quad (2)$$

$$\phi(1) = 0 \quad (3)$$

where a is the contact radius between the probe and the sample, δ is the probe indentation depth, h is the distance from the top of the layer to the interface with the substrate (height of the layer), E_1 is the Young's modulus and ν_1 is the Poisson's ratio of the layer, F is the indentation force, and β is a function of f (Supplementary Table 1):

$$\beta(t) = t\int_0^t \frac{f'(ra)}{\sqrt{t^2 - r^2}}dr \quad (4)$$

where $0 < r < 1$. Here ϕ is an intermediate function to reduce the system of dual integral equations to a single equation and is related to the stress profile of the indentation. The kernel K is smooth and defined by

$$K(x,t) = 2\int_0^\infty H(2u)\cos\left(\frac{a}{h}tu\right)\cos\left(\frac{a}{h}xu\right)du \quad (5)$$

with

$$H(u) = -\frac{d + g(1+u)^2 + 2dge^{-u}}{e^u + d + g(1+u^2) + dge^{-u}} \quad (6)$$

$$d = \frac{(3-4\nu_1) - \mu(3-4\nu_2)}{1+\mu(3-4\nu_2)} \quad (7)$$

$$g = \frac{1-\mu}{\mu + 3 - 4\nu_1} \quad (8)$$

$$\mu = \frac{E_1(1+\nu_2)}{E_2(1+\nu_1)} \quad (9)$$

where E_2 and ν_2 are the Young's modulus and Poisson's ratio of the substrate. When $E_1 = E_2$ or $h \to \infty$, Eq. (1) is reduced to the homogeneous case considered by Sneddon.[22] Eq. (1) is numerically solved[39] simultaneously with the boundary condition Eq. (3) to determine a and ϕ, then F is calculated using Eq. (2). In the case of an indentation onto a two-layer sample with a stiffer substrate (E_2>E_1), F will be larger compared an indentation onto a sample with homogeneous E_1, and similarly for a sample with a softer substrate (E_2<E_1), F will be smaller compared to homogenous E_1 (Fig. 1B). The relationship between a and δ varies in the same way as F; for a stiffer substrate, a will be larger than the homogeneous case, and a will be smaller for a softer substrate (Fig. 1C). The substrate effect is strongest for ν=0.5 and weakens as ν decreases (Fig. S1). This formalism does not model an asymptotic relationship in F when δ>h, especially in the case of E_2>E_1, thus we ensure that δ<h henceforth. Dhaliwal and Rau present a series approximation[37] for ϕ and we observed that this will provide a similar result as Nyström interpolation[39] for E_2>E_1 but converges slowly when E_1>E_2 (Fig. S2).

Additionally, the surface deformation profile u_z of the layer as a function of lateral distance from the probe is[37]

$$u_z^1\left(r;\frac{r}{a}>1\right) = \frac{2}{\pi}\int_0^1 \frac{\delta-\beta(x)}{\sqrt{(r/a)^2-x^2}}dx - \frac{4\left(1-{\nu_1}^2\right)}{\pi^2 E_1 h}\int_1^{r/a}\frac{dy}{\sqrt{(r/a)^2-y^2}}\int_0^1 K(y,t)\phi(t)dt \quad (10)$$

(for r/a < 1, the surface strain is the difference of the probe shape and indentation). The surface deformation profile depends on the elastic mismatch; the deformation at higher lateral distances from the probe will increase as E_2 decreases (Fig. 1D).

Solving the above equations will calculate F and a as a function of the other physical parameters (f, δ, h, E_1, E_2, ν_1, ν_2) thus providing a template to fit experimental F-δ data. The formalism has recently been used to deconvolute the Young's modulus of the layer E_1 using Eq. 1-9 by pre-computing a table of correction factors to the Young's modulus for an AFM dataset in which f is known, δ is constant, F is measured, ν_1=ν_2=0.5 is assumed, and h and E_2 are independently measured.[16] We denote E_0 as the apparent Young's modulus which is obtained by fitting the F-δ to a standard contact model (e.g. the Hertz model) and pre-compute a table of values of dimensionless corrections to the apparent Young's modulus E_1/E_0 as a function of the first layer height h and relative elastic mismatch E_1/E_2. Once the table is generated, it may be iteratively interpolated to find the unknown Young's modulus E_1 of the layer. This method directly solves Eq. (1-9) to deconvolute one of the Young's moduli, however it lacks generality and is computationally expensive as a separate table must be generated for each experimental condition and curve fitting method (for example constraints on the contact point). Thus, we seek to use numeric results of Eq. (1-9) to provide a more intuitive framework for understanding the substrate effect in the indentation problem.

Materials and methods

Finite element analysis

Finite element analysis was performed using ANSYS Workbench 14.0. The models assume axial symmetry around the center of the indenting probe. The indenting probe was modeled as a sphere of radius 5 μm with much higher rigidity (~GPa) than the samples being indented (~kPa-MPa). The sample was modeled as two bonded elastic (isotropic) layers each with $\nu_1 = \nu_2 = 0.49$ ($\nu = 0.49$ was chosen as opposed to 0.5 for numeric stability). The layer had variable height (4 μm or 20 μm) and fixed Young's modulus (100 kPa) and the substrate had a fixed height of 200 μm and variable Young's modulus (100 Pa-100 MPa) and both layers had a radius of 150 μm. The material was fixed at the bottom of the second layer and had a triangular mesh size of 100 nm which and tapers to larger values at a distance of 25 μm from the probe. The probe used a triangular mesh size of 50 nm and the contact between the tip and sample was frictionless. The probe was then moved into the sample in 2 nm increments and the force response was calculated at the interface between the probe and sample, thus producing a simulated F-δ curve which are copied to MATLAB for analysis.

PDMS preparation and atomic force microscopy

Polydimethylsiloxane (PDMS, Sylgard 184, Dow Corning) was mixed with base:crosslinker ratios of 25:1 and 40:1 and degassed. Thin PDMS layers were spin-coated at 4000 rpm for 2 min onto silanized (Methyltrichlorosilane, Sigma Aldrich) glass coverslips (Gold Seal 48mm×60mm, Electron Microscopy Sciences) and thick (~3 mm) PDMS substrates were poured onto glass-bottom petri dishes and cured at

65°C overnight. The layer thicknesses were determined by the interference pattern of the back reflected light at the gel interfaces using a confocal microscope (Microtime 200, PicoQuant) at 6 locations on the gel used to form the layer; thickness values represent the mean ± standard deviation. Both layers were then cleaned in oxygen plasma (PDC-001, Harrick Plasma) for 2 min, pressed together to bond, and then the silanized coverslip was removed to produce a layered PDMS substrate. AFM measurements were performed using an MFP-3D-BIO (Asylum Research) with a 10 μm diameter glass bead glued to a tipless cantilever (ACT-TL, AppNano) with stiffness 57 N/m as determined from the thermal tuning method. Experiments were performed at room temperature and in 2% bovine serum albumin in phosphate buffered saline to reduce tip-sample adhesion. The probe velocity was 2 μm/s and indentation depths up to 1.5 μm were analyzed. Data is collected from multiple indentations at different locations on a single two-layered sample as well the homogeneous stiffness samples prepared at the same time (gels within a single figure panel were prepared at the same time, gels in different figure panels were not); stiffness values represent the mean ± standard deviation from at least 48 indentations per sample.

PDMS preparation and macroindentation

PDMS was mixed with base:crosslinker ratios of 10:1 and 25:1, degassed, and cured at 65°C overnight. Bulk indentation measurements were performed with an Anton-Paar MCR302. A steel bead with a diameter of 9.53 mm was glued to a disposable measuring plate (D-PP25/AL/S07) using epoxy. The rheometer was programmed to adjust the gap distance relative to the bottom of the gel (equivalent to δ with an offset) and the resulting normal force is measured resulting in a F-δ curve. Measurements were performed in air. The height of the PDMS gel was determined from the contact point of the rheometer. F-δ curve and indentation depths up to 1.5 mm were analyzed. Data is collected from a single indentation on a single layered sample as well the homogeneous stiffness samples prepared at the same time.

Data analysis

F-δ curves are analyzed using home-built routines in MATLAB (R2015b, MathWorks). For all data using a spherical indenter, data is fit using linear least squares regression on the Hertz model with a fully constrained contact point (the fits contain $F = 0$, $\delta = 0$). Contact points were manually chosen in a point-and-click scheme. Eq. (1) is solved using the MATLAB program Fie.[39] Built-in MATLAB functions trapz and quadv are used for numeric integration and lsqcurvefit for curve fitting. Wolfram Mathematica 8.0 is used to solve Eq. (4). The Poisson's ratio was assumed to be 0.5.

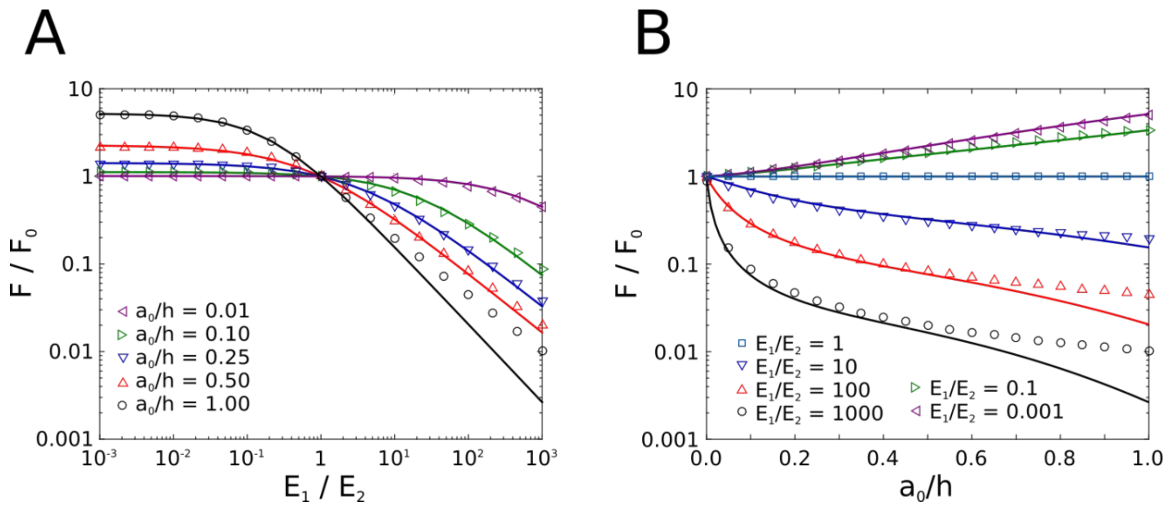

Figure 2: Results of the two-layer model for F/F_0 for a parabolic (Hertz model) probe. (A) F/F_0 as a function of E_1/E_2 for various values of a_0/h (magenta a_0/h=0.01, green 0.10, blue 0.25, red 0.50, and black 1.00). (B) The same data as (A) except showing F/F_0 as a function of a_0/h for various values of E_1/E_2 (cyan E_1/E_2=1, blue 10, red 100, black 1000, green 0.1, and magenta 0.001). Open markers indicate the solution to Eq. (1-9) while solid lines indicate the solution to Eq. (16).

Results

The deconvolution method

In elastic contact mechanics, F is linearly proportional to E and has some non-linear dependence on δ. We denote F_0 and a_0 as the force and contact radius between the probe and sample for the homogeneous case of E_1 (see also Supplementary Table 1), so for the Hertz model[21]

$$F_0 = \frac{E_1}{(1-\upsilon_1{}^2)}\frac{4}{3}\sqrt{R\delta^3} \quad (11)$$

$$a_0 = \sqrt{R\delta} \quad (12)$$

where R is the apex radius of the probe. In the two-layer model, E is replaced by E_1, and h and E_2 are introduced as additional multiplicative term describe the contribution of the substrate and perturbs F (and a) from the case of homogeneous E_1. In Eq. (1-9), h and E_2 only appear in terms relative to the contact radius a and E_1, respectively. Therefore, when the Poisson's ratios of the layer and substrate are known (here we assume ν_1=ν_2=0.5 for incompressible materials), the indentation into the two-layer material can be described as an indentation into the layer treated as a homogeneous material E_1 with an extra corrective term from substrate. The perturbative term should have dependence on the relative height to the probe size and contact radius a_0/h and the elastic mismatch E_1/E_2, both of which are dimensionless.

We calculated deviations from the homogeneous case F/F_0 for a values of E_1/E_2 in the range of 10^{-3} to 10^3 and $a_0/h<1$ for a parabolic (Hertz model) indenter (Fig. 2A, B). When $E_1<E_2$, $F/F_0>1$ and the substrate effect saturates for increasing E_2, indicating an upper limit of E_2 altering the F-δ response. When $E_1>E_2$, $F/F_0<1$ and the effect diverges for decreasing E_2 and the F-δ response becomes dominated by the rigidity of the substrate. These effects are amplified as a_0/h increases. We also calculated F/F_0 for various E_1/E_2 and a_0/h for other common axisymmetric indenter geometries: a cone (Sneddon model[22]), hyperbola,[38] and cone with a spherical cap (sphero-cone,[16] Supplementary Table 1), and these are similar for each geometry (Fig. S3).

The shape of F/F_0 for the 3D axisymmetric indentation is similar to the 1D problem of compressing springs with stiffnesses k_1 with k_2 in series (Supplementary Text); in the regime of $k_2>>k_1$ the force required saturates to compress only k_1 without the second spring, and in the regime of $k_1>>k_2$ a power law emerges (Eq. S3). We phenomenologically extend the 1D solution to the full 3D solution using Eq. (1-9) and assuming $\nu_1=\nu_2=0.5$ to take the form of

$$F \approx F_0 \frac{B\left(\frac{a_0}{h}\right) + 1}{B\left(\frac{a_0}{h}\right)\left(\frac{E_1}{E_2}\right)^{A\left(\frac{a_0}{h}\right)} + 1} \qquad (13)$$

where $0 \leq A \leq 1$ is the power law behavior in the elastic mismatch and B is the saturation point at $E_1<<E_2$, both of which depend on the 3D geometry a_0/h. In the 1D case of two springs in series, $A=B=1$. We fit the data in Fig. 2 to Eq. (13) as a function of E_1/E_2 and subsequently fit A and B as functions of a_0/h to obtain (Supplementary Note 1, Fig. S4)

$$A\left(\frac{a_0}{h}\right) \approx \min\left(1, 0.72 - 0.34\left(\frac{a_0}{h}\right) + 0.51\left(\frac{a_0}{h}\right)^2\right) \quad (14)$$

$$B\left(\frac{a_0}{h}\right) \approx 0.85\left(\frac{a_0}{h}\right) + 3.36\left(\frac{a_0}{h}\right)^2 \quad (15)$$

These satisfy $F=F_0$ when $E_1=E_2$ or $a_0/h=0$ and $F\approx F_0\, E_2/E_1$ when $a_0>>h$. The value and interpretation of B is similar to other layered indentation models with a rigid substrate ($E_2=\infty$).[26] Eq. (14-15) are valid only for a_0/h < 1 (Fig. S4C) and errors arise for large a_0/h and $E_1>>E_2$. Eq. (14-15) were approximated for a parabolic (Hertz model) indenter, however the numeric coefficients will be similar for other indenter shapes up to $a_0/h\sim0.5$. Thus, we can write a final equation to approximately fit experimental F-δ data using a spherical or parabolic indenter on a two-layered sample as

$$F \approx \frac{16E_1\sqrt{R\delta^3}}{9}\left(\frac{0.85\left(\frac{a_0}{h}\right) + 3.36\left(\frac{a_0}{h}\right)^2 + 1}{\left(0.85\left(\frac{a_0}{h}\right) + 3.36\left(\frac{a_0}{h}\right)^2\right)\left(\frac{E_1}{E_2}\right)^{0.72 - 0.34\left(\frac{a_0}{h}\right) + 0.51\left(\frac{a_0}{h}\right)^2} + 1}\right) \quad (16)$$

where, $\nu_1=\nu_2=0.5$ is assumed, $\delta<h$, and $a_0/h<1$. Eq. (16) as written provides a similar result as numerically solving Eq. (1-9) to within 8% for $a_0/h<0.8$ and $E_2>10E_1$, or $a_0h<0.5$ and $E_2>100E_1$ (Fig. 2). F depends on all parameters (E_1, E_2, and h) and the effects of changing one variable may be similar to changing another; thus, fitting for multiple unknown parameters in Eq. (16) may result in overfitting of the data and errors in determining any of the input parameters will propagate into further errors in fitting for the unknown parameters. Henceforth in this article, fitting for either E_1 or E_2 is performed when the other modulus is known and h is always known (single unknown parameter fitting).

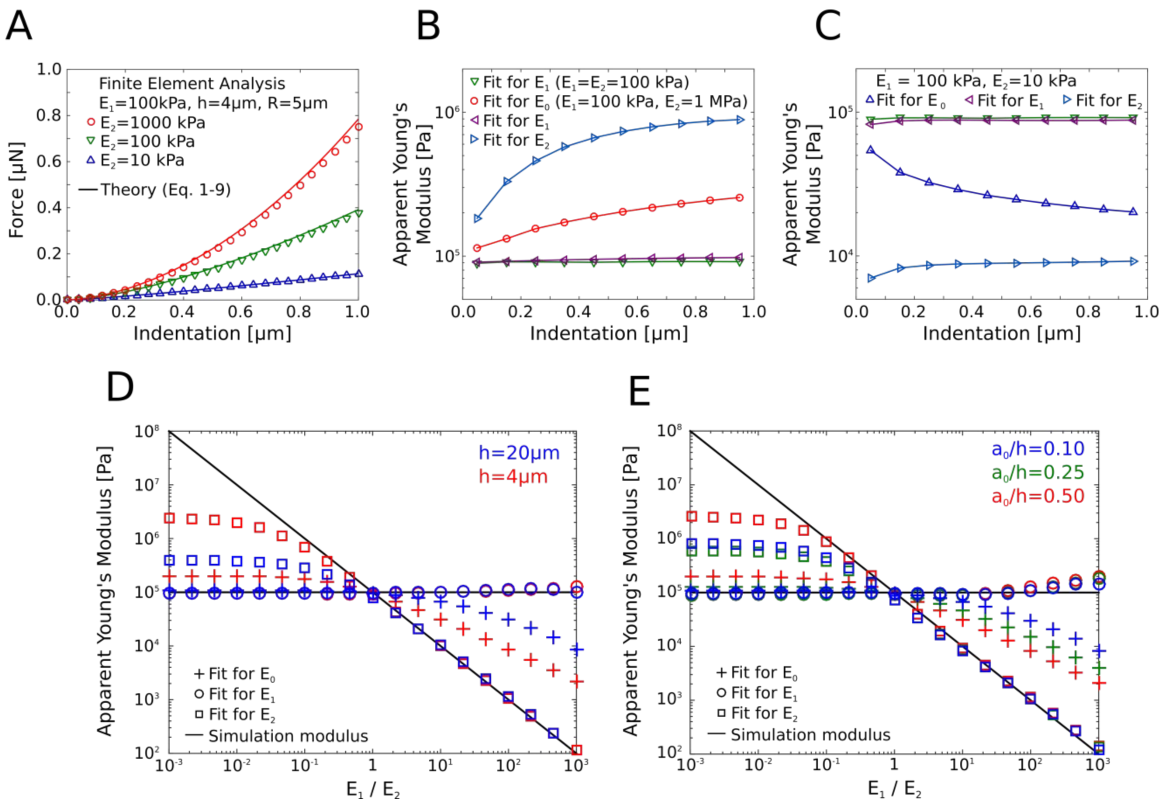

Figure 3: Finite element analysis validation of the two-layer indentation model. (A) F-δ curves generated from the numeric model for the homogeneous case (green), a softer substrate (blue, $E_2=E_1/10$), and a stiffer substrate (red, $E_2=10E_1$), and the corresponding F-δ curves calculated from Eq. (1-9) (solid lines). Parameters used are E_1=100 kPa, h=4 μm, R=5 μm, δ=1.0 μm, and $\nu_1=\nu_2=0.49$. (B) Fits for the Young's modulus of a layered material with a stiff substrate ($E_2=10E_1$), including the Hertz model fit (red), the fit for the layer E_1 (magenta), the fit for the substrate E_2 (cyan), and the fit for the layer E_1 of a homogeneous material (green). (C) Same as (B) for a layered material with a soft substrate ($E_2=E_1/10$). (D) Deconvolutions of finite element analysis data using precomputed correction tables. Plus signs show fits using the standard Hertz model E_0, circles are two-layer fits for the layer E_1 which is kept constant at 100 kPa, squares are fit for the substrate E_2 which is variable (simulation moduli shown in black), blue denotes a thicker layer (h=20 μm), red denotes a thinner layer (h=4 μm). (E) Deconvolutions of finite element analysis data by performing a least squares fit on Eq. (14), using the same legend as (C) with δ up to a_0/h=0.10, a_0/h=0.25, and a_0/h=0.50 in blue, green, and red, respectively.

Validation of the method with simulated F-δ curves

To test the validity of the model, we performed finite element analysis simulations of an indentation into a layered elastic material using a spherical probe. We simulated *F-δ* data for two different layer heights (20 μm and 4 μm, corresponding to a_0/h=0.11 and a_0/h=0.56, respectively, for a spherical probe with R=5 μm and δ=1 μm) with varying E_2 and constant E_1 (Fig. 3C). We observed good agreement in the *F-δ* curves generated by finite element analysis and the two-layer model Eq. (1-9) for the same geometric and material parameters (Fig. 3A) and in the surface displacement profile of the layer with Eq. (10) (Fig. S5). When we fit the F-δ curves on a layered material to the Hertz model to determine E_0, we observe a dependence of the fitted (apparent) Young's modulus value with indentation depth (Fig. 3B, C). Fitting F-δ data using Eq. (16) for E_1, removes the depth-dependence of the Young's modulus and we can recover the value of the layer in the simulation. Furthermore, fitting the F-δ data using Eq. 16 for E_2 provides mixed results; when E_1>E_2 we are able to recover the value of E_2 in the simulation (Fig. 3C), however when E_1>E_2 we are only able to recover the value at high indentation depths (Fig. 3B). This is due to the fact that F/F_0 will plateau at a certain value of a_0/h even if E_2 is further increased (Fig. 2A).

We next fit for the Young's moduli of the two layers from finite element models for different combinations of E_1/E_2 and a_0/h (Fig. 3D, E). In the case of an indentation into a thick (h=20 μm) layer, the standard Hertz model is able to accurately estimate the layer Young's modulus in the case of E_2>E_1, however for E_1>E_2, large errors arise which scale with decreasing E_2. When the layer height is thin (h=4 μm), errors arise in estimating the Young's modulus using the Hertz model when E_2>E_1 and are more pronounced for E_1>E_2 (Fig. S6A). When we directly used Eq. (1-9) as a template to fit the simulated finite element data (Fig. 3D), we obtained E_1 for nearly all h and E_2, and E_2 for E_2<E_1 within 20% accuracy, however E_2 could not be estimated when E_1<E_2 due to the saturating effect on F/F_0 with increasing E_2.

The deconvolution results for the approximate method Eq. (16) (Fig. 3E, S6B) provides similar results however with less accuracy for large a_0/h and small E_2; E_1 has errors within ~20% when the elastic mismatch is within two orders of magnitude and a_0/h<0.25, and E_2 cannot be determined when E_2>E_1. Errors in determining E_1 in the regime of E_1>E_2 become larger than the exact method Eq. (1-9) as E_2 decreases and a_0/h increases.

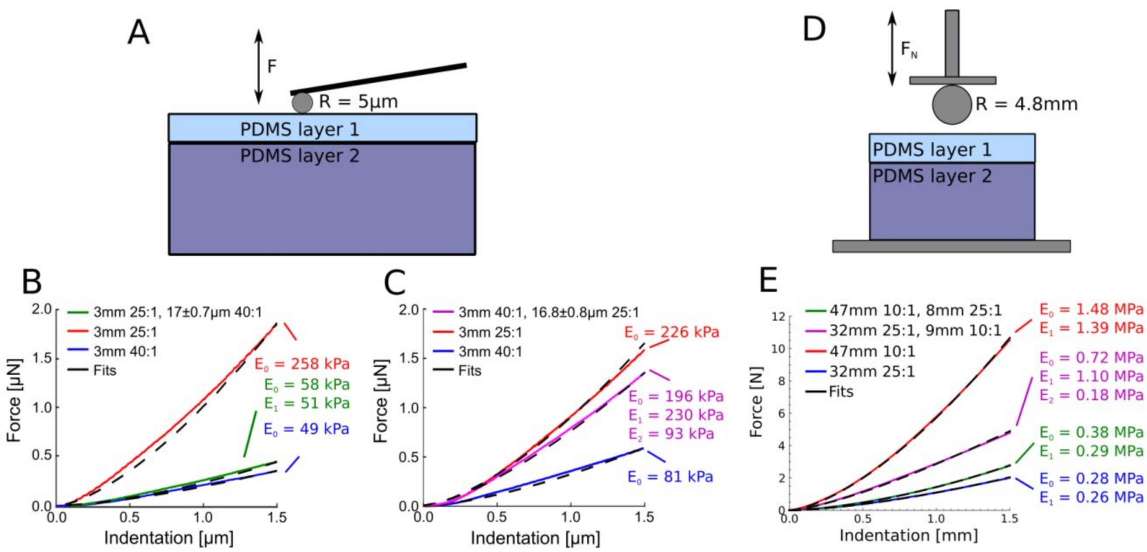

Figure 4: Experimental indentation-based measurements of layered PDMS gels. (A) Schematic of AFM indentation of a layered PDMS gel. (B) *F*-δ curves of a soft layer and rigid substrate (green), a homogenous soft gel (blue), and a homogenous stiff gel (red). Fits are shown using Hertz model (E_0, in black) for the homogenous gels, and the two-layer model (E_1, in black) with known substrate and the substrate modulus (E_2) with known layer height. (C) *F*-δ curves for a stiff layer and soft support (magenta) and similar analysis as in B. The two-layer model was used to fit for the layer modulus (E_1) when the substrate modulus and layer height are known, and is also used to fit the substrate modulus (E_2) when the layer modulus and layer height are known. (D) Schematic of macroindentation on a layered PDMS gel. (E) *F*-δ curves showing rheometer data for single-layered gels and double-layered gels with the respective Young's modulus values from fitting.

Demonstration of the deconvolution method with experimental F-δ curves

In order to test the efficacy of the model in analyzing experimental *F*-δ data, we fabricated layered PDMS samples with stiffness mismatch (base:crosslinker ratios of 25:1 and 40:1 for stiff on soft, respectively) and performed AFM-based microindentation (Fig. 4A) with a spherical probe (Fig. S7). Here we measure the Young's moduli of both layers independently and the layer thickness using the interference patterns of the back reflected light at the interfaces (h~17 μm and δ=1.5 μm, thus a_0/h~0.16). Once the modulus of each homogenous gel had been independently determined, we tested if we could use Eq. (16) to deconvolute each constituent modulus in a layered sample when one of E_1, E_2, or h is fitted for and the other two are treated as known input parameters. In the case of a soft layer with stiff substrate (E_1<E_2), we observe that the force is higher than the homogenous soft gel and less than the homogenous stiff gel (Fig. 4B), thus fitting with the Hertz model for E_0 (58 ± 6 kPa) provides a result different from both (258 ± 8 kPa and 49 ± 4 kPa for 25:1 and 40:1, respectively). When the force-indentation curve on the layered gel is fit with Eq. (16) with known substrate E_2 (the value of E_0 of the homogeneous stiff gel) and h, the fitted value E_1 (51 ± 5 kPa) of the layer is in good agreement with the homogenous stiffness E_0 of the soft gel. We do not fit for E_2 as we observed that fitting for E_2 in the case of a stiff substrate with a relatively low a_0/h results in high errors in determining E_2.

The effect is similar for the case of a stiff layer and soft substrate (Fig. 4C); the E_0 fits for these samples differ from both homogenous gels (196 ± 15 kPa, 226 ± 5 kPa, and 81 ± 3 kPa for layered, 25:1, and 40:1, respectively). However, when E_2 (E_0 of the homogenous soft gel) and h are used as input parameters in Eq. (16), the fitted value E_1 (230 ± 22 kPa) is similar to E_0 of the stiff gel. When E_1 (E_0 of the homogenous stiff gel) and h are used as input parameters in Eq. (16), the fitted E_2 (93 ± 29 kPa) is similar to E_0 of the soft gel.

As the model is applicable to any length scale, we additionally performed macroindentation experiments on layered PDMS gels using a steel bead (R = 4.8 mm) glued to the measuring plate of a rheometer (Fig. 4D). We collected F-δ data on two-layered and single-layered PDMS gels with crosslinking ratio of 10:1 and 25:1 and fit the data using Eq. (14) (Fig. 4E). Indentations were first performed on homogenous PDMS gels and we obtained Young's moduli E_1 of 1.39 and 0.26 MPa for 10:1 and 25:1 crosslinking ratios, respectively. Thin ($h \sim 9$ mm and δ = 1.5 mm, thus $a_0/h \sim 0.3$) slices of additional PDMS gel were attached on top of the thick gels and additional F-δ data (Fig. 4E) was collected. As qualitatively expected, the force of indentation on a thin 10:1 gel with a 25:1 substrate is lower than the force of indentation on a homogeneous 10:1 gel, and the force of indentation on a thin 25:1 gel with a 10:1 substrate is higher than the force of indentation on a homogeneous 25:1 gel. Fits for E_0 using the Hertz model gave results that are significantly different from the homogenous gel stiffnesses (0.72 MPa for 10:1 on top of 25:1; 0.38 MPa for 25:1 on top of 10:1). When the F-δ data is analyzed using Eq. (16), the fit for E_1 of the layered gels gives values comparable to those measured on the bulk gels (1.10 and 0.29 MPa for 10:1 and 25:1 thin layers, respectively). In the case of the thin 10:1 gel on the 25:1 gel substrate, because E_2<E_1

it is possible to fit for E_2, and we obtained 0.18 MPa for the thick 25:1 substrate beneath the 10:1 thin layer. Taken together, these experiments serve as a proof-of-principle for using the model presented here in quantitatively analyzing F-δ curves on elastic layered samples.

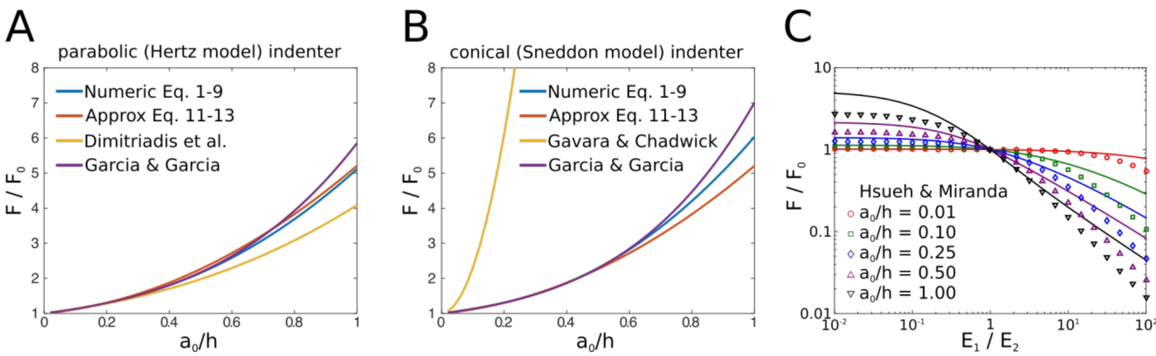

Figure 5: Comparison of F/F_0 with other layered models. (A) The case of a parabolic indenter and a rigid substrate; blue shows the numeric solution of Eq. (1-9), red shows Eq. (16), yellow shows the model by Dimitriadis et al.,[27] and magenta shows the model by Garcia and Garcia.[26] (B) The case of a conical indenter and a rigid substrate; blue shows the numeric solution Eq. (1-9), red shows Eq. (16), yellow shows the model by Gavara and Chadwick,[28] and magenta shows the model by Garcia and Garcia.[26] (C) The case of a parabolic indenter and a two-layer substrate as a function of E_1/E_2; open markers indicate the model by Hsueh and Miranda[30] and solid lines indicate Eq. (1-9) with a_0/h values of 0.01 (red), 0.10 (green), 0.25 (blue), 0.50 (magenta), and 1.00 (black).

Discussion

Indentations into bonded two-layered elastic systems are treated as indentation into a homogeneous layer with an additional perturbative term that depends on E_1/E_2 and a_0/h and summarized as Eq. (16). Qualitatively, the force of indentation scales in a similar manner to springs in series. For a stiffer substrate ($E_2>E_1$), the effect of the substrate will increase with a_0/h but will saturate for higher values of E_2, and the saturation point will depend on the value of a_0/h. In this scenario, the dominant factor in the perturbative term is a_0/h, which directly relates to the indentation depth. For a softer substrate ($E_2<E_1$), there is a power-law relationship between F/F_0 and E_1/E_2. In this scenario, both E_1/E_2 and a_0/h strongly affect F/F_0.

The two-layer model presented here may be used as a quantitative guide during the design and analysis of AFM indentation experiments with biological samples. If elastic heterogeneity is known or suspected (for example a mammalian cell with stiff actomyosin cortex,[25] a thin cell or polymer gel, or a cell seeded on soft extracellular matrix[16, 40]), E_1/E_2 and a_0/h may be roughly estimated and Eq. (16) will predict two-layer effects on F. Depending on the scientific question being addressed, a_0 can be tuned by changing δ or the indenter geometry. If the goal is to quantify the rigidity of the layer (E_1), using low a_0/h will help to ensure that the layer dominates the F-δ response. If the goal is the measure the rigidity of the substrate (E_2), then increasing a_0 will make the F-δ response more characteristic of E_2 (Fig. 2, S4C), however the model presented here is inaccurate for E_2>>E_1 and another approach where δ>h would be more suitable, such as in Kaushik et al.[19] As the two-layer effect depends on all of the sample parameters (h, E_1, E_2) as well as the indentation parameters (f, δ) (Fig. 2), it may be necessary to accurately and independently measure several of these parameters or perform further experiments on the same sample using different probe geometries in order to accurately determine the unknown parameter. For a practical example, it has been observed that a cell's Young's modulus measured by AFM depends on the geometry of the probe, with sharper probes resulting in larger values.[18, 25] As the substrate effect scales with the contact radius, the two-layer model corroborates observations that sharper conical probes are more sensitive than larger bead probes to the stiffer actomyosin cortex than the cell body.[25]

In Hertzian contact with a parabolic indenter there is power-law scaling $F \propto \delta^{3/2}$, however if a second layer is present then this power-law behavior is changed; for $E_2>E_1$ the exponent will be effectively higher and for $E_2<E_1$ it will be lower (Fig. 1B). If an experimental F-δ curve bends from the expected power-law behavior and the fitted elastic modulus depends on indentation depth (as in Fig. 2B, C) then mechanical heterogeneity may be present; the two-layer model provides guidelines for interpreting this data.

Other analytical models have been independently derived in the case of indentations onto thin samples with a rigid substrate. The model presented here provides similar corrective terms as Dimitriadis et al.[27] and Garcia and Garcia,[26] although differ from Gavara and Chadwick[28] (Fig. 5A, B). Both the two-layer model here and by Garcia and Garcia[26] observe a direct dependence of both F and a on a_0/h for multiple probe geometries. We also compared our two-layer model with another derived by Hsueh and Miranda[30] and find that the corrective terms agree only for small stiffness mismatches (Fig. 5C). It should be noted that Eq. 16 was approximated to examine the substrate effects on indenting the top layer, analogous to a "bottom-effect correction". When $E_2<<E_1$ or $a_0/h>1$, the force becomes more characteristic of the substrate (e.g. the top layer effects on indenting the substrate) and Eq. (16) is no longer accurate (Fig. S4C). Future work could be performed to improve the phenomenological approach in Eq. (13-16) to account for the asymptotic switch between the two mismatched layers, such as in Korsunsky and Constantinescu.[32]

Finally, the model also predicts that, as E_2 decreases, the shape of the deformed surface of the layer will change such that positions further away from the probe will undergo higher displacement. This also means that the 3D strain field induced by a deformation when $E_2 < E_1$ will be larger than the homogeneous case. The two-layer model presented here is only valid when the substrate (an elastic half-space) and the layer have infinite lateral dimensions. However, based on the surface displacement Eq. (10), the model predicts that the effects on F from a finite-sized sample will be amplified when $E_2<E_1$.

Conclusions

We describe a simple method for the quantitative mechanical analysis of two-layered elastic materials and anticipate that our results will yield to more precise quantification of heterogeneous soft matter and biological specimens. This model may be easily applied to the design, analysis, and interpretation of AFM indentation experiments and may also be used as a general description of elastic contact mechanics regarding the correlation of length scales and stiffness in the presence of external forces and deformations. Considerations for future improvements include quantitative effects of lateral sample size and viscous and non-linear effects of layered materials.

Acknowledgements

This work was supported by the grants NIH/NCI U54CA143862 and NSF #1510700 to R.R., and NSF IIA-14115018 to B.L.D..

References

1. D. T. N. Chen, Q. Wen, P. A. Janmey, J. C. Crocker and A. G. Yodh, *Annual Review of Condensed Matter Physics*, 2010, **1**, 301-322.
2. P. J. de Pablo, I. A. Schaap, F. C. MacKintosh and C. F. Schmidt, *Physical review letters*, 2003, **91**, 098101.
3. C. Carrasco, A. Luque, M. Hernando-Perez, R. Miranda, J. L. Carrascosa, P. A. Serena, M. de Ridder, A. Raman, J. Gomez-Herrero, I. A. Schaap, D. Reguera and P. J. de Pablo, *Biophysical journal*, 2011, **100**, 1100-1108.

4. M. Hernando-Perez, R. Miranda, M. Aznar, J. L. Carrascosa, I. A. Schaap, D. Reguera and P. J. de Pablo, *Small*, 2012, **8**, 2366-2370.
5. J. Domke and M. Radmacher, *Langmuir*, 1998, **14**, 3320-3325.
6. A. Navaei, H. Saini, W. Christenson, R. T. Sullivan, R. Ros and M. Nikkhah, *Acta biomaterialia*, 2016, **41**, 133-146.
7. N. Peela, F. S. Sam, W. Christenson, D. Truong, A. W. Watson, G. Mouneimne, R. Ros and M. Nikkhah, *Biomaterials*, 2016, **81**, 72-83.
8. J. Candiello, T. S. P. Grandhi, S. K. Goh, V. Vaidya, M. Lemmon-Kishi, K. R. Eliato, R. Ros, P. N. Kumta, K. Rege and I. Banerjee, *Biomaterials*, 2018, **177**, 27-39.
9. H. Saini, K. R. Eliato, C. Silva, M. Allam, G. Mouneimne, R. Ros and M. Nikkhah, *Cellular and molecular bioengineering*, 2018, **11**, 419-433.
10. M. Radmacher, M. Fritz, C. M. Kacher, J. P. Cleveland and P. K. Hansma, *Biophysical journal*, 1996, **70**, 556-567.
11. R. E. Mahaffy, C. K. Shih, F. C. MacKintosh and J. Kas, *Physical review letters*, 2000, **85**, 880-883.
12. S. E. Cross, Y. S. Jin, J. Rao and J. K. Gimzewski, *Nature nanotechnology*, 2007, **2**, 780-783.
13. J. Solon, I. Levental, K. Sengupta, P. C. Georges and P. A. Janmey, *Biophysical Journal*, 2007, **93**, 4453-4461.
14. J. Rother, H. Noding, I. Mey and A. Janshoff, *Open biology*, 2014, **4**, 140046.
15. A. Fuhrmann, J. R. Staunton, V. Nandakumar, N. Banyai, P. C. Davies and R. Ros, *Physical biology*, 2011, **8**, 015007.
16. J. R. Staunton, B. L. Doss, S. Lindsay and R. Ros, *Scientific reports*, 2016, **6**, 19686.
17. O. Jonas, C. T. Mierke and J. A. Kas, *Soft Matter*, 2011, **7**, 11488-11495.
18. P. H. Wu, D. R. Aroush, A. Asnacios, W. C. Chen, M. E. Dokukin, B. L. Doss, P. Durand-Smet, A. Ekpenyong, J. Guck, N. V. Guz, P. A. Janmey, J. S. H. Lee, N. M. Moore, A. Ott, Y. C. Poh, R. Ros, M. Sander, I. Sokolov, J. R. Staunton, N. Wang, G. Whyte and D. Wirtz, *Nature methods*, 2018, **15**, 491-498.
19. G. Kaushik, A. Fuhrmann, A. Cammarato and A. J. Engler, *Biophysical journal*, 2011, **101**, 2629-2637.
20. M. Plodinec, M. Loparic, C. A. Monnier, E. C. Obermann, R. Zanetti-Dallenbach, P. Oertle, J. T. Hyotyla, U. Aebi, M. Bentires-Alj, R. Y. Lim and C. A. Schoenenberger, *Nature nanotechnology*, 2012, **7**, 757-765.
21. H. Hertz, *J. Reine Angew. Math.*, 1882, **92**, 156-171.
22. I. N. Sneddon, *Int. J. Engng. Sci.*, 1965, **3**, 47-57.
23. D. C. Lin and F. Horkay, *Soft Matter*, 2008, 669-682.
24. R. E. Mahaffy, S. Park, E. Gerde, J. Kas and C. K. Shih, *Biophysical journal*, 2004, **86**, 1777-1793.
25. R. Vargas-Pinto, H. Gong, A. Vahabikashi and M. Johnson, *Biophys J*, 2013, **105**, 300-309.
26. P. D. Garcia and R. Garcia, *Biophysical journal*, 2018, **114**, 2923-2932.
27. E. K. Dimitriadis, F. Horkay, J. Maresca, B. Kachar and R. S. Chadwick, *Biophysical journal*, 2002, **82**, 2798-2810.
28. N. Gavara and R. S. Chadwick, *Nature nanotechnology*, 2012, **7**, 733-736.
29. G. Huajian, C. Cheng-Hsin and L. Jin, *International Journal of Solids and Structures*, 1992, **29**, 2471-2492.
30. C.-H. Hsueh and P. Miranda, *Journal of Materials Research*, 2004, **19**, 94-100.
31. H. Xu and G. M. Pharr, *Scripta Materialia*, 2006, **55**, 315-318.
32. A. M. Korsunsky and A. Constantinescu, *Thin Solid Films*, 2009, **517**, 4835–4844.
33. Y. Abidine, A. Constantinescu, V. M. Laurent, V. Sundar Rajan, R. Michel, V. Laplaud, A. Duperray and C. Verdier, *Biophysical journal*, 2018, **114**, 1165-1175.
34. E. U. Azeloglu, G. Kaushik and K. D. Costa, *Conf. Proc. IEEE Eng. Med. Biol. Soc.*, 2009, **978**, 4273–4276.
35. S. Iyer, R. M. Gaikwad, V. Subba-Rao, C. D. Woodworth and I. Sokolov, *Nature nanotechnology*, 2009, **4**, 389-393.
36. Y. Ding, J. Wang, G. K. Xu and G. F. Wang, *Soft Matter*, 2018, **14**, 7534-7541.
37. R. S. Dhaliwal and I. S. Rau, *Int J Eng Sci*, 1970, **8**, 843-&.
38. B. B. Akhremitchev and G. C. Walker, *Langmuir*, 1999, **15**, 5630-5634.

39. K. E. Atkinson and L. F. Shampine, *ACM Transactions on Mathematical Software*, 2008, **34**.
40. J. Solon, I. Levental, K. Sengupta, P. C. Georges and P. A. Janmey, *Biophysical journal*, 2007, **93**, 4453-4461.